Journal of Zhejiang University-SCIENCE B (Biomedicine & Biotechnology)
ISSN 1673-1581 (Print); ISSN 1862-1783 (Online)
www.jzus.zju.edu.cn; www.springerlink.com
E-mail: jzus@zju.edu.cn

Comparative transcriptomic analysis reveals adriamycin-induced apoptosis via p53 signaling pathway in retinal pigment epithelial cells*#

Yu-chen LIN[1,2], Ze-ren SHEN[1,2], Xiao-hui SONG[1,2], Xin LIU[1,2], Ke YAO[†‡1,2]

[1]*Eye Center, the Second Affiliated Hospital, Zhejiang University School of Medicine, Hangzhou 310009, China*

[2]*Key Laboratory of Ophthalmology of Zhejiang Province, Hangzhou 310009, China*

[†]E-mail: xlren@zju.edu.cn

Received July 30, 2018; Revision accepted Sept. 28, 2018; Crosschecked Nov. 16, 2018

Abstract: Objective: This paper applied a transcriptomic approach to investigate the mechanisms of adriamycin (ADR) in treating proliferative vitreoretinopathy (PVR) using ARPE-19 cells. Methods: The growth inhibitory effects of ADR on ARPE-19 cells were assessed by sulforhodamine B (SRB) assay and propidium iodide (PI) staining using flow cytometry. The differentially expressed genes between ADR-treated ARPE-19 cells and normal ARPE-19 cells and the signaling pathways involved were investigated by microarray analysis. Mitochondrial function was detected by JC-1 staining using flow cytometry and the Bcl-2/Bax protein family. The phosphorylated histone H2AX (γ-H2AX), phosphorylated checkpoint kinase 1 (p-CHK1), and phosphorylated checkpoint kinase 2 (p-CHK2) were assessed to detect DNA damage and repair. Results: ADR could significantly inhibit ARPE-19 cell proliferation and induce caspase-dependent apoptosis in vitro. In total, 4479 differentially expressed genes were found, and gene ontology items and the p53 signaling pathway were enriched. A protein–protein interaction analysis indicated that the TP53 protein molecules regulated by ADR were related to DNA damage and oxidative stress. ADR reduced mitochondrial membrane potential and the Bcl-2/Bax ratio. *p53*-knockdown restored the activation of c-caspase-3 activity induced by ADR by regulating Bax expression, and it inhibited ADR-induced ARPE-19 cell apoptosis. Finally, the levels of the γ-H2AX, p-CHK1, and p-CHK2 proteins were up-regulated after ADR exposure. Conclusions: The mechanism of ARPE-19 cell death induced by ADR may be caspase-dependent apoptosis, and it may be regulated by the p53-dependent mitochondrial dysfunction, activating the p53 signaling pathway through DNA damage.

Key words: Adriamycin; Proliferative vitreoretinopathy; Retinal pigment epithelial; p53; Apoptosis
https://doi.org/10.1631/jzus.B1800408 **CLC number:** R3

1 Introduction

Proliferative vitreoretinopathy (PVR) is a very common complication that causes recurrent retinal detachment and requires complicated surgery. Current surgical treatments for PVR include removing the traction and peeling the sub-retinal and epiretinal membranes (Claes and Lafetá, 2014), but there are still a high recurrence rate of 4%–34% (Charteris et al., 2002; Heimann et al., 2007; Leiderman and Miller, 2009) and severe complications. The affected eyes may suffer from permanent vision loss (Eibl et al., 2009; Claes and Lafetá, 2014). Therefore, developing a novel pharmacological strategy for preventing PVR and for assisting surgical therapy is of great interest.

‡ Corresponding author
* Project supported by the Zhejiang Province Key Research and Development Program (No. 2015C03042), China
# Electronic supplementary materials: The online version of this article (https://doi.org/10.1631/jzus.B1800408) contains supplementary materials, which are available to authorized users
ORCID: Yu-chen LIN, https://orcid.org/0000-0002-2679-2849; Ke YAO, https://orcid.org/0000-0002-6764-7365

The most important cell types in the PVR pathogenesis are retinal pigment epithelium (RPE) cells, which de-differentiate and migrate through a retinal break and proliferate on the retinal surface (Machemer et al., 1978). RPE cells have been widely used in PVR pathogenesis studies.

In the past few decades, efforts have been made to find antineoplastic agents from conventional antitumor drugs to treat PVR. For example, it was demonstrated that Taxol helped reduce the incidence of detachment in experimental PVR models (van Bockxmeer et al., 1985; Daniels et al., 1990). Some studies reported no consistent benefits from using 5-fluorouracil in preventing postoperative PVR in patients (Asaria et al., 2001; Charteris et al., 2004; Wickham et al., 2007). In addition, an in vitro study identified methotrexate as capable of reducing the growth of PVR cells (Amarnani et al., 2017). A randomized controlled trial that included 286 eyes with preoperative stage C2 or advanced PVR showed that although daunorubicin does not promote anatomical healing of the retina, it helps to improve the rate of retinal reattachment and reduce the rate of secondary surgery (Wiedemann et al., 1998). In another study, 30 patients with stage D1 PVR received vitreoretinal surgery with an intravitreal injection of daunorubicin. The results indicated an increased rate of retinal attachment and improved visual acuity after three months of follow-up (Kumar et al., 2002). The above research revealed that human PVR is amenable to pharmacologic treatment and several anti-cancer drugs may have promising characteristics for preventing PVR.

Adriamycin (ADR, or doxorubicin), which is a 14-hydroxylated version of daunorubicin, is produced by daunorubicin through a biosynthetic pathway and is an anthracycline-based drug like daunorubicin. ADR is widely used to treat various cancers, such as leukemia, lymphoma, breast cancer, and soft tissue sarcomas (Minotti et al., 2004; Lisenko et al., 2017; Patel et al., 2017; Zhao et al., 2017). Compared with daunorubicin, ADR is more widely used and more effective for cancer treatment (di Marco et al., 1969). The antitumor function of ADR involves the apoptosis regulator Bcl-2, phosphatase, and tensin homolog, Wnt, protein kinase C, tumor necrosis factor, and signal molecules for the autophagosome marker LC3-II (Wang J et al., 2013; Dash et al., 2015; Wang ZC et al., 2015; Martins-Neves et al., 2016; Xu et al., 2017; Zhao et al., 2017). ADR has also been identified as a potential medication to treat PVR because of its antiangiogenic and anti-proliferative properties (Sunalp et al., 1984, 1985; Steinhorst et al., 1993; Rong and Li, 2002; Kuo et al., 2007). ADR demonstrated the inhibition of fibroblast proliferation and the prevention of membrane formation in a rabbit model of PVR (Sunalp et al., 1984). Moreover, ADR in microspheres was investigated as a new modality for PVR treatment (Moritera et al., 1992). Intravitreal injections of ADR are safe at a concentration of approximately 23 μmol/L, significantly decreasing vitreous and retinal proliferative responses (Rong and Li, 2002). ADR is well known in tumor cells, and it has been shown to be a potentially effective modality for PVR therapy, but few studies have explored the mechanism of action in human RPE cells. To understand the efficacy or side effects of ADR for PVR treatment and the relationship between RPE cells and ADR, studying the mechanisms of ADR's pharmacological effects on PVR is necessary.

Thus, the present study aimed to perform a microarray analysis to determine differentially expressed genes (DEGs) among cultured human RPE cells (ARPE-19) treated and untreated with ADR, and to investigate the cellular apoptosis induced by DNA damage and the p53-dependent mitochondrial pathway in ARPE-19 cells.

2 Materials and methods

2.1 Cell culture

The human RPE cell line (ARPE-19) was derived from the American Type Culture Collection. Frozen ARPE-19 cells were rapidly thawed (<1 min) in a 37 °C water bath and then slowly diluted and cultured with a pre-warmed Dulbecco's modified Eagle medium/nutrient mixture F-12 Ham (DMEM/F12; Hyclone, Logan, UT, USA) containing 20% fetal bovine serum (FBS) and 50 U penicillin/50 μg/ml streptomycin in 60-mm dishes (Corning Ltd., Lowell, MA, USA). The dishes were placed in an incubator with 5% CO_2 at 37 °C. The cellular density was 5×10^5 cells/ml, and the medium was changed daily during the first 5 d. ARPE-19 cells were confluent after 3 d and became hyperconfluent after 5 d. The cells were trypsinized

and transferred from 60-mm dishes to 100-mm dishes (about 1:2 expansion) and then cultured under the same atmosphere in a DMEM/F12 medium (Hyclone) containing 10% FBS and 50 U penicillin/50 μg/ml streptomycin. The medium was changed daily and cells were passaged every other day.

2.2 Reagents

ADR was kindly provided by the First Affiliated Hospital, Zhejiang University School of Medicine (Hangzhou, China). Dimethyl sulfoxide (DMSO), propidium iodide (PI), sulforhodamine B (SRB), 4',6-diamidino-2-phenylindole (DAPI), 5,5',6,6'-tetrachloro-1,1',3,3'-tetraethylbenzimidazol carbocyanine iodide (JC-1), Tris-Base, and trichloroacetic acid were obtained from Sigma-Aldrich (St. Louis, USA). ADR was dissolved in DMSO and stored at −20 °C. In all experiments, the final DMSO solvent concentration was <0.2%. Primary antibodies directed against β-actin, glyceraldehyde 3-phosphate dehydrogenase (GAPDH), p53, Bcl-2, Bcl-2-associated X (Bax), and horseradish peroxidase (HRP)-labelled secondary antibodies were obtained from Santa Cruz Biotechnology (CA, USA). Antibodies directed against phosphorylated histone H2AX (γ-H2AX), cleaved poly(ADP-ribose) polymerase (c-PARP), cleaved caspase-3 (c-caspase-3), phosphorylated checkpoint kinase 1 (p-CHK1), and phosphorylated checkpoint kinase 2 (p-CHK2) were purchased from Cell Signaling Technology (MA, USA).

2.3 Microarray analysis

Total RNA was isolated from ARPE-19 cells in the control group and the three groups treated with 1, 2, and 4 μmol/L ADR for 24 h (one sample per group) using TRIzol (Life Technologies) following the manufacturer's instructions. An Agilent microarray (8×60K; Agilent, Palo Alto, CA, USA) was used for cell signaling selection.

Total RNA was purified using the RNeasy Mini kit (Qiagen, Chatsworth, CA, USA) and RNase-free DNase set (Qiagen, Chatsworth, CA, USA). Cyanine-3 (Cy3)-labelled cRNA was prepared from 0.2 μg RNA using the One-Color Low RNA Input Linear Amplification PLUS kit (Agilent) according to the manufacturer's instructions, followed by RNeasy column purification (Qiagen, Valencia, CA, USA). The dye incorporation and cRNA yield were checked with a NanoDrop ND-1000 spectrophotometer. A sample of 0.6 μg Cy3-labelled cRNA (specific activity >10.0 pmol Cy3/μg cRNA) was fragmented at 60 °C for 30 min in a reaction volume of 22.5 μl containing 1× Agilent fragmentation buffer and 2× Agilent blocking agent following the manufacturer's instructions. Upon completion of the fragmentation reaction, 22.5 μl 2× Agilent hybridization buffer was added to the fragmentation mixture and hybridized to OE Human lncRNA Microarray V4.0 (Agilent) for 17 h at 65 °C in a rotating Agilent hybridization oven. After hybridization, microarrays were washed with GE Wash Buffer 1 (Agilent) for 1 min at room temperature and with GE Wash Buffer 2 (Agilent) for 1 min at 37 °C; they were immediately dried by brief centrifugation. Slides were immediately scanned after washing on the Agilent DNA Microarray Scanner (G2505C) using the one color scan setting for 4×180K array slides (scan area 61.0 mm×21.6 mm, scan resolution 3 μm, dye channel set to green, and green photomultiplier tube gain (PMT) set to 100%). The scanned images were analyzed with Feature Extraction software version 10.7.1.1 (Agilent) using the default parameters to obtain the background-subtracted, spatially detrended processed signal intensities as the raw data, which were normalized into a quantile algorithm with Genespring 13.0 (Agilent). The probe profile showed that at least one out of two samples flagged as "detected" was maintained. For the ARPE-19 cell line, the control group and three groups treated with ADR were analyzed. The raw data were submitted to the National Center of Biotechnology Information (NCBI) website (http://www.ncbi.nlm.nih.gov/geo, accession number GSE104662).

2.4 DEGs and functional analysis

Significant DEGs between the control group and the three ADR-treated groups were identified according to the criteria of a $\log_2$-fold change of >2. A hierarchical clustering analysis was performed to visualize DEGs using a Venn diagram and heat map via the Venny 2.1 (http://bioinfogp.cnb.csic.es/tools/venny) and MEV 4.6.0 software.

The Kyoto Encyclopedia of Genes and Genomes (KEGG) pathway enrichment analysis and gene ontology (GO) analysis were performed based on the database of OmicsBean (http://www.omicsbean.com:88). Only KEGG pathways with P values of <0.05 were selected.

The public database STRING (Version 10.5, http://string-db.org) was used to generate protein–protein interaction networks, and protein–protein interactions with a combined score higher than the median value of all combined scores were selected. The interaction networks were visualized using Cytoscape (Version 3.5.1).

2.5 Cell proliferation of ARPE-19 cells detected with SRB assay

ARPE-19 cells were seeded at 3×10^4 per well in 96-well plates (Corning) and cultured for one day in growth media until confluent. Cells were exposed to 1 and 2 μmol/L ADR for 24 h and 2 μmol/L ADR for 24, 48, and 72 h, and they were then fixed with 0.1 g/ml trichloroacetic acid and stained with SRB. The cells were dissolved in the same amount of 10 mmol/L Tris-Base, and measured at 510 nm using a multi-well spectrophotometer. Cell viability was calculated for each well according to the following formula: $[1-(A_{510,\ \text{control cells}}-A_{510,\ \text{treated cells}})/A_{510,\ \text{control cells}}]\times100\%$, where A_{510} is the absorbance at 510 nm.

2.6 Detection of the apoptosis in ARPE-19 cells by flow cytometry

Apoptotic rates were measured by PI dye. After exposure to 0, 1, and 2 μmol/L ADR for 72 h and 2 μmol/L ADR for 0, 24, 48, and 72 h, cells were harvested and fixed with 70% ethanol at −20 °C overnight. The cells were re-suspended in 500 μl of phosphate-buffered saline (PBS) containing 50 μg RNase at 37 °C for 30 min, and then 5 μg PI was added. The solution was maintained in the dark. Each measurement contained 10000 cells, and apoptotic rates were detected with a FACSCalibur cytometer (BD, Bioscience, San Jose, CA, USA).

2.7 siRNA transfection

Small interfering ribonucleic acid (siRNA) (GenePharma Co. Ltd., Shanghai, China) was used to knock down the *p53* gene expression in ARPE-19 cells. The sequence of *p53* siRNA was 5'-GCATC TTATCCGAGTGGAA-3'. Cells were seeded in 6-well plates (2×10^5 per well) and cultured for one day in growth media until confluent. Then, *p53* siRNA or non-targeting siRNA was transfected using Oligofectamine 2000 (Invitrogen, 12252-011, Carlsbad, CA, USA) according to the instructions, and 2 μmol/L ADR was added to the plates. After exposure to 2 μmol/L ADR for 24 or 72 h, the cells were centrifuged at 3000*g* for 3–5 min and re-suspended in lysis buffer containing 150 mmol/L NaCl, 50 mmol/L Tris-HCl, 2 mmol/L ethylenediaminetetraacetic acid (EDTA), 2 mmol/L ethylene glycol-bis(β-aminoethyl ether)-*N*,*N*,*N*',*N*'-tetraacetic acid (EGTA), 25 mmol/L NaF, 25 mmol/L β-sodium glycerophosphate, 0.3% Triton X-100, 0.3% NP-40, 0.25% leupeptin, 0.1% phenylmethylsulfonyl fluoride (PMSF), and 0.1% $NaVO_3$. Western blot assay was used to measure the expression levels of p53, c-PARP, and c-caspase-3 in cells exposed to 2 μmol/L ADR for 72 h and Bax proteins in cells exposed to 2 μmol/L ADR for 24 h.

2.8 Measurement of DNA damage with the γ-H2AX assay

ARPE-19 cells were cultured onto glass culture slides and treated with 1 and 2 μmol/L ADR for 6 h. The control group was not treated with ADR. Cells were washed twice with PBS and fixed with 4% paraformaldehyde for 20 min at room temperature. Subsequently, cells were permeabilized with PBS containing 0.1% Triton X-100. After blocking with 4% bovine serum albumin (BSA) for 30 min, the cells were incubated with the primary γ-H2AX antibody (Cell Signaling Technology, MA, USA) overnight. Cells were washed with PBS and then incubated with secondary antibodies (Invitrogen, Carlsbad, CA, USA) for 1 h. The fluorescence intensity of γ-H2AX was quantified with the ImageJ software to validate DNA double-strand (DDS) breaks.

2.9 Measurement of mitochondrial membrane potential using JC-1 assay

ARPE-19 cells in 6-well plates were treated with either vehicle or 1 and 2 μmol/L ADR at 37 °C for 24 h. The cells were harvested and washed with 500 μl PBS three times and then centrifuged at 1500*g* for 5 min. The cells were re-suspended in 500 μl PBS and then incubated with 10 μg/ml JC-1 dye at room temperature for 30 min in the dark. Subsequently, the samples were centrifuged at 1500*g* for 5 min and the supernatant was discarded. The cells were re-suspended in 1 ml PBS, and fluorescence was measured using a FACSCalibur cytometer (BD, Bioscience, San Jose, CA, USA). Each measurement involved 5000 events.

2.10 Western blot analysis

ARPE-19 cells were harvested after treatment with ADR. The cell suspensions were centrifuged at 3000*g* for 3–5 min and resuspended in the lysis buffer. Protein concentration was determined by a Lowry protein assay kit (Thermo Fisher Scientific, Rockford, IL, USA). In total, 20 μg of protein lysates were resolved by sodium dodecyl sulfate-polyacrylamide gel electrophoresis (SDS-PAGE) on 10% gels and then transferred to polyvinylidene difluoride (PVDF) membranes (Millipore, Billerica, MA, USA). The membranes were blocked with 5% non-fat dry milk in PBS with 0.1% Tween for 1 h at room temperature and then incubated overnight at 4 °C with primary antibodies against β-actin (1:1000 in 1% BSA; Santa Cruz Biotechnology, CA, USA), GAPDH (1:1000 in 1% BSA; Santa Cruz Biotechnology), p53 (1:1000 in 1% BSA; Santa Cruz Biotechnology), Bcl-2 (1:500 in 1% BSA; Santa Cruz Biotechnology), Bax (1:1000 in 1% BSA; Santa Cruz Biotechnology), γ-H2AX (1:1000 in 1% BSA; Cell Signaling Technology), c-PARP (1:1000 in 1% BSA; Cell Signaling Technology), c-caspase-3 (1:1000 in 1% BSA; Cell Signaling Technology), p-CHK1 (1:1000 in 1% BSA; Cell Signaling Technology), and p-CHK2 (1:1000 in 1% BSA; Cell Signaling Technology). Subsequently, the membranes were washed and incubated for 1 h at room temperature with 1:10000 HRP-conjugated anti-mouse, anti-goat, or anti-rabbit IgG (Santa Cruz Biotechnology) as the secondary antibody. Proteins were visualized on autoradiography film with a Western blot analysis detection system (ECL Plus; Amersham Biosciences Inc., NJ, USA) and detected quantitatively by densitometry using the QuantityOne software (Bio-Rad). β-actin and GAPDH were used as inner references, and the ratio of Bcl-2/Bax was calculated.

2.11 Statistical analysis

The results were expressed as the mean±standard deviation (SD). A Student's *t*-test was employed to compare the difference between the ADR-treated group and the untreated control. Statistical significance among the groups was analyzed by one-way analysis of variance (ANOVA) using the Stata 14.0 software (StataCorp, Texas, USA) and it was considered acceptable at a level of $P<0.05$. Statistical analysis and graphics were performed using Prism software (GraphPad Software, San Diego, USA).

3 Results

3.1 Cell proliferation of ARPE-19 cells as detected with SRB assay

Fig. 1a shows that the cellular viabilities were (82.6±1.0)% and (76.5±0.9)% in ARPE-19 cells exposed to 1 and 2 μmol/L ADR for 24 h, respectively, which were significantly lower than those (100%) in the controls ($P<0.001$), indicating the dose-effect relationship. Fig. 1b indicates that the cellular viabilities ((76.5±0.9)%, (45.3±3.8)%, and (9.8±1.9)%, respectively) in ARPE-19 cells exposed to 2 μmol/L ADR for 24, 48, and 72 h significantly decreased with ADR exposure time, and there were significant differences in cellular viabilities among the four different time-points ($P<0.001$). Fig. 1c demonstrates that the ADR-treated cells exhibited the features of cell death, including shrinkage and detachment from the vessel surface.

3.2 Apoptosis and caspase activity in ARPE-19 cells exposed to ADR

Figs. 2a and 2b show that in ARPE-19 cells exposed to 0, 1, and 2 μmol/L ADR for 72 h, the apoptotic rates were (0.36±0.29)%, (18.39±3.70)%, and (63.19±4.98)%, respectively, and these increased in a concentration-dependent manner. Furthermore, there were significant differences in apoptotic rates among the three groups ($P<0.01$ or $P<0.001$). Figs. 2c and 2d indicate that the apoptotic rates induced by 2 μmol/L ADR at 0, 24, 48, and 72 h were (0.44±0.23)%, (4.96±0.83)%, (45.96±4.64)%, and (63.19±4.98)%, respectively, and these increased with the exposure time. There were significant differences in the apoptotic rates among the four time-points ($P<0.01$ or $P<0.001$).

Figs. 2e, 2g, and 2h show that the expression levels of c-PARP and c-caspase-3 proteins in ARPE-19 cells exposed to 1 and 2 μmol/L ADR for 72 h were significantly enhanced ($P<0.01$). Moreover, the pan-caspase inhibitor Z-VAD-FMK could reduce the expression levels of c-PARP and c-caspase-3 proteins in ARPE-19 cells exposed to 2 μmol/L ADR ($P<0.05$; Figs. 2f, 2i, and 2j).

3.3 Target gene prediction and pathway analysis

To predict the target genes that accelerate ADR-related ARPE-19 cell death, a microarray was conducted to analyze the mRNA expression levels in

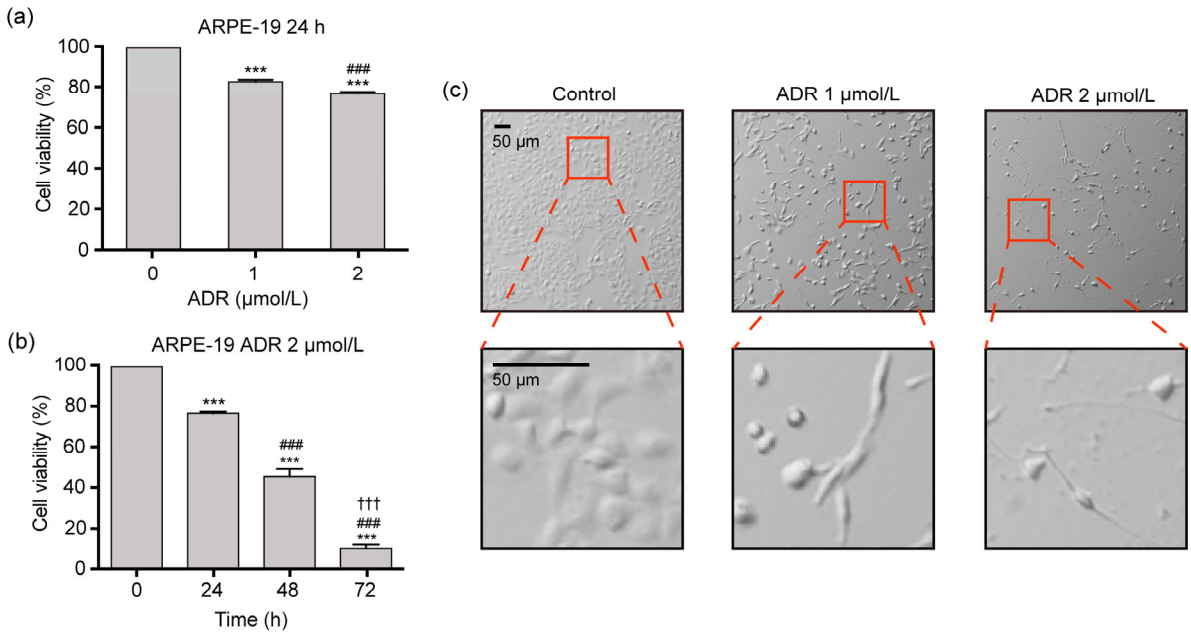

Fig. 1 Cell viability and morphology of ARPE-19 cells exposed to ADR in the SRB assay

(a) Cell viability in ARPE-19 cells exposed to 0, 1, and 2 μmol/L ADR for 24 h. (b) Cell viability in ARPE-19 cells exposed to 2 μmol/L ADR for 0, 24, 48, and 72 h. (c) Cell morphology in ARPE-19 cells exposed to 1 and 2 μmol/L ADR for 48 h. Data are expressed as mean±SD (n=3). $^{***}P$<0.001, as compared with the control group; $^{###}P$<0.001, as compared with the 1 μmol/L ADR group or 2 μmol/L ADR for 24 h group; $^{†††}P$<0.001, as compared with the 2 μmol/L ADR for 48 h group

ADR-treated and normal ARPE-19 cells. Genes with a fold change of more than two were considered as DEGs. In total, 18891 DEGs were found expressed in the control and ADR-treated ARPE-19 cells, among which, 4479 (23.7%) genes were co-expressed in the 1, 2, and 4 μmol/L ADR groups (Fig. 3a). Subsequently, a hierarchical clustering analysis was performed, and a heat map of the correlation coefficients among the 4479 altered gene expression profiles was used to represent the fold change ratios (Fig. 3b). The results indicated that samples treated with 1 and 2 μmol/L ADR showed significantly different expression profiles from those in the control group. Therefore, the 1 and 2 μmol/L gene profiles were selected for further study.

The list of 6539 DEGs co-expressed in the 1 and 2 μmol/L ADR groups was imported to the KEGG and GO databases through OmicsBean for a functional enrichment analysis. The top 10 significantly impacted KEGG pathways are listed (Fig. 3c). The data show that the p53 signaling pathway was most significantly impacted by ADR treatment, with a $-\log P$ of 3.36 (P<0.05). According to the results of GO analysis, DEGs were mainly involved in the binding category (Fig. S1).

The protein–protein interaction of DEGs in the p53 signaling pathway was visualized using Cytoscape. The genes highlighted in the protein–protein network revealed that ADR treatment regulated genes mainly concerned with the TP53 protein. The interactions among TP53-related proteins are illustrated in Fig. 3d, revealing that the important proteins in the networks belonged to DNA damage and oxidative stress.

3.4 Expression levels of proteins related to the p53 signaling pathway

Western blot analysis determined that the protein levels of p53 in ARPE-19 cells exposed to 1 or 2 μmol/L ADR for 24 h were significantly higher than those in the control group (P<0.05 or P<0.01, Figs. 4a and 4b). Figs. 4c and 4d reveal that the apoptotic rate of ARPE-19 cells exposed to 2 μmol/L ADR was significantly higher than that of the control group and that of ARPE-19 cells exposed to 2 μmol/L ADR plus siRNA (P<0.001). Figs. 4e–4h show that the levels of the c-PARP, c-caspase-3, and p53 proteins decreased

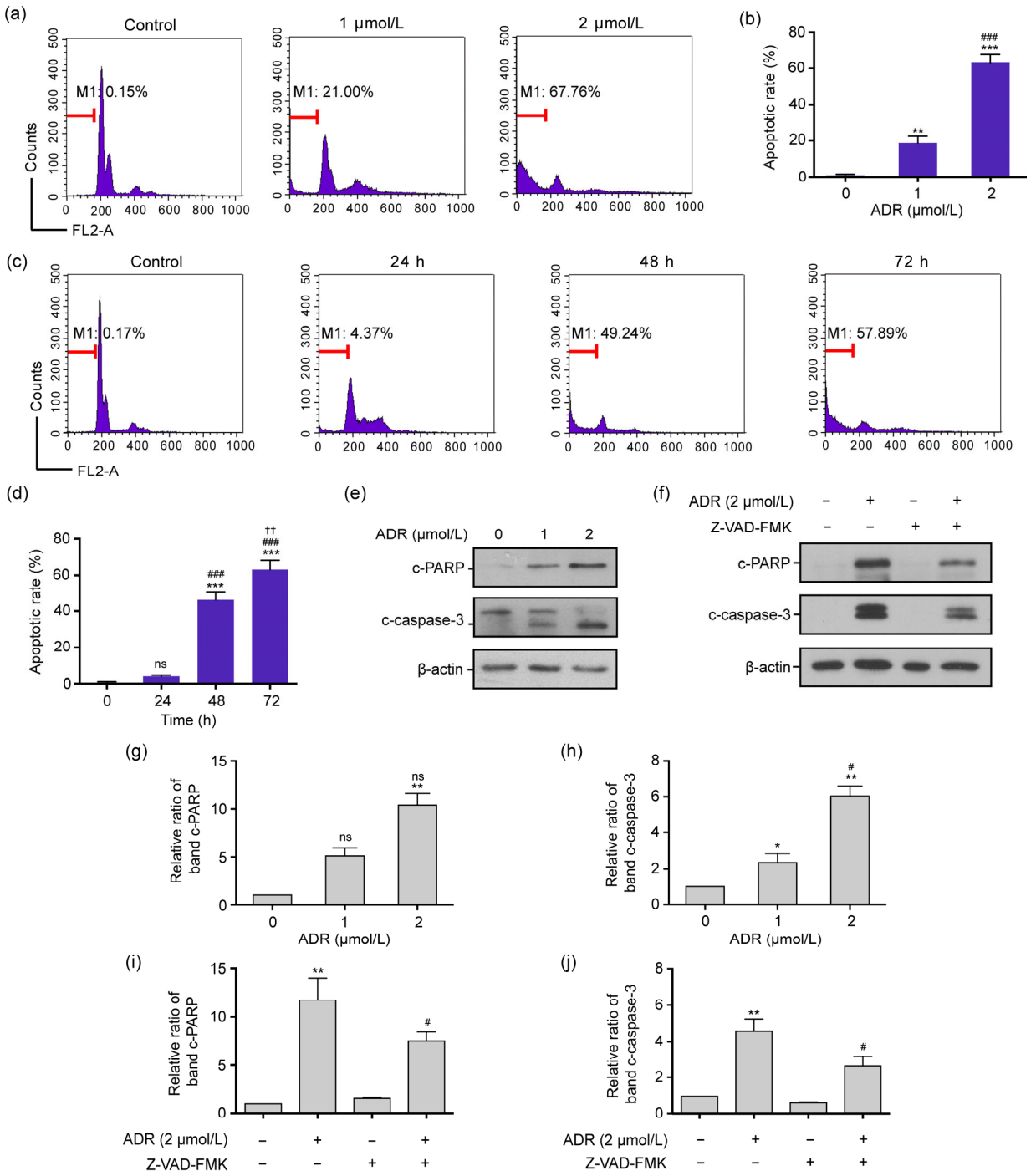

Fig. 2 Apoptosis and the expression levels of the c-caspase-3 and c-PARP proteins of ARPE-19 cells exposed to ADR in flow cytometry and Western blot assay

(a, b) The apoptotic rates in ARPE-19 cells exposed to 0, 1, and 2 μmol/L ADR for 72 h by flow cytometry. (c, d) The apoptotic rates in ARPE-19 cells exposed to 2 μmol/L ADR for 0, 24, 48, and 72 h. (e, g, h) The expression levels of c-PARP and c-caspase-3 proteins in ARPE-19 cells exposed to 0, 1, and 2 μmol/L ADR for 72 h. (f, i, j) The expression levels of c-PARP and c-caspase-3 proteins in ARPE-19 cells exposed to 2 μmol/L ADR and 2 μmol/L ADR plus 20 μmol/L Z-VAD-FMK for 72 h. Data are expressed as mean±SD (n=3). $^{*}P$<0.05, $^{**}P$<0.01, $^{***}P$<0.001, as compared with the control group; $^{\#}P$<0.05, $^{\#\#}P$<0.01, $^{\#\#\#}P$<0.001, as compared with the 1 μmol/L ADR for 72 h, 2 μmol/L ADR for 24 h, and 2 μmol/L ADR for 72 h groups; $^{\dagger\dagger}P$<0.01, as compared with the 2 μmol/L ADR for 48 h group; ns (not significant): 1 μmol/L ADR or 24 h vs. control, or 2 μmol/L ADR vs. 1 μmol/L ADR

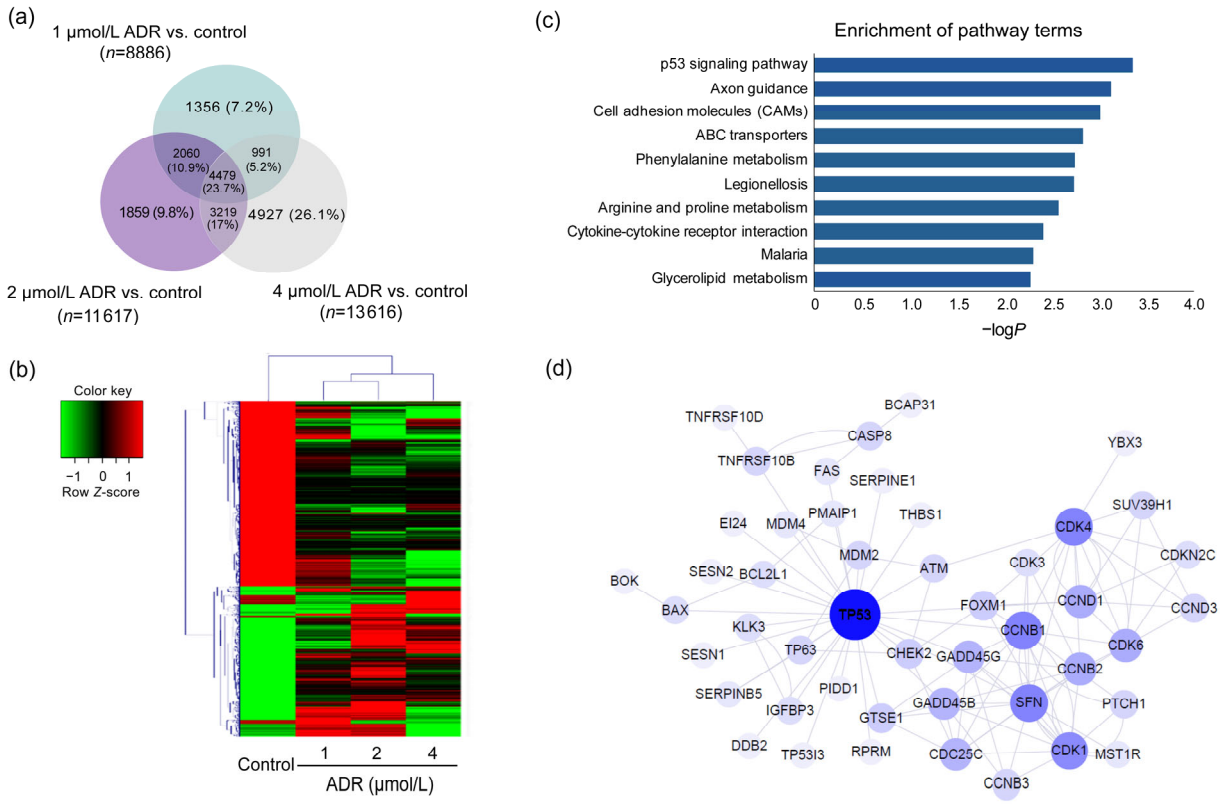

Fig. 3 DEGs in the control group and ARPE-19 cells exposed to ADR

(a) Results of a Venn diagram analysis of the differentially expressed genes identified from the control and ADR-treated groups. (b) A heat map of hierarchical clustered genes. In total, 4479 genes from the genomics data showed a significantly aberrant expression (at least 2-fold change), $P<0.05$. In the clustering analysis, red and green regions indicate the up-regulated and down-regulated genes, respectively. (c) An enrichment analysis of the top 10 pathways for DEGs based on the KEGG database. The horizontal and vertical axes represent the enrichment score of –log$P$ and the pathway category, respectively. (d) The network represents the correlations between TP53-related genes. Large and small node sizes represent high and low relevance, respectively. Lines were defined as the interaction of the genes

in ARPE-19 cells exposed to 2 μmol/L ADR plus *p53* siRNA for 72 h, as compared with those only exposed to 2 μmol/L ADR for 72 h ($P<0.05$ or $P<0.01$).

3.5 Mitochondrial apoptosis in ARPE-19 cells exposed to ADR

The occurrence of mitochondrial apoptosis induced by ADR was measured by JC-1 assay. The results (Figs. 5a and 5b) show that, as compared with the control group, the mitochondrial apoptosis based on the green fluorescence intensity ratio in ARPE-19 cells exposed to 1 and 2 μmol/L ADR for 24 h was significantly enhanced ($P<0.01$ or $P<0.001$). Moreover, Figs. 5c–5e demonstrate that in ARPE-19 cells exposed to 1 and 2 μmol/L ADR for 24 h, the expression levels of the anti-apoptotic proteins Bcl-2 and Bax decreased and increased, respectively, when compared with those in the control group ($P<0.05$). Compared with the control group, the ratio of Bcl-2/Bax significantly declined in the 2 μmol/L ADR-treated group ($P<0.05$; Fig. 5f).

3.6 Mitochondrial pathway associated with the inhibition of ADR-induced apoptosis in *p53* siRNA-treated ARPE-19 cells

The results of the JC-1 assay (Fig. 5) confirmed that mitochondrial apoptosis was involved in ADR-related RPE apoptosis. Moreover, a network analysis (Fig. 3d) revealed that genes related to mitochondria, *Bax*, and *Bcl2L1* correlate with the p53 signaling pathway. To elucidate the mechanism of the inhibition

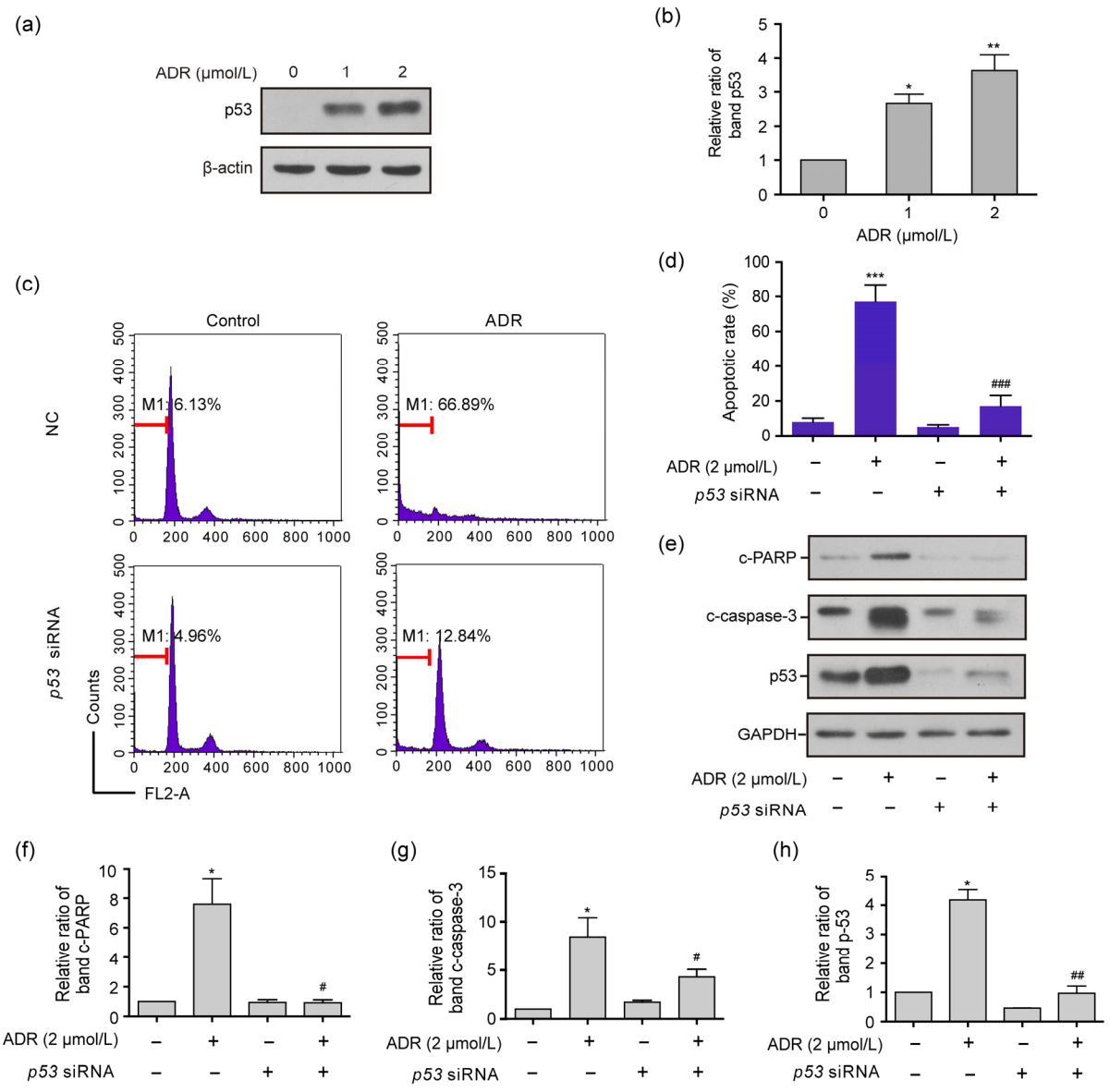

Fig. 4 Apoptotic rates and expression levels of c-PARP, c-caspase-3, and p53 proteins in ARPE-19 cells exposed to ADR, *p53* siRNA, and ADR plus *p53* siRNA

(a, b) The p53 expression levels in RPE cells exposed to 1 and 2 μmol/L ADR for 72 h. (c, d) The apoptotic rates of ARPE-19 cells exposed to ADR, *p53* siRNA and ADR plus *p53* siRNA for 72 h by flow cytometry. (e–h) The expression levels of the c-PARP, c-caspase-3, and p53 proteins for each above subgroup in the Western blot assay. Data are expressed as mean±SD (n=3). $^{*}P$<0.05, $^{**}P$<0.01, $^{***}P$<0.001, as compared with the control group; $^{\#}P$<0.05, $^{\#\#}P$<0.01, $^{\#\#\#}P$<0.001, as compared with the 2 μmol/L ADR group

of *p53* siRNA-mediated ARPE-19 cell apoptosis induced by ADR, the level of the mitochondrial apoptosis-associated protein Bax was assessed by Western blot assay. Fig. 6 demonstrates that the Bax protein expression level in ARPE-19 cells exposed to 2 μmol/L ADR for 24 h was significantly higher than that in ARPE-19 cells exposed to non-targeting siRNA and 2 μmol/L ADR plus *p53* siRNA for 24 h (P<0.01 or P<0.001).

3.7 γ-H2AX assay and the protein expression of γ-H2AX, p-CHK1, and p-CHK2

The results of a network analysis (Fig. 3d) revealed that the important proteins related to the TP53

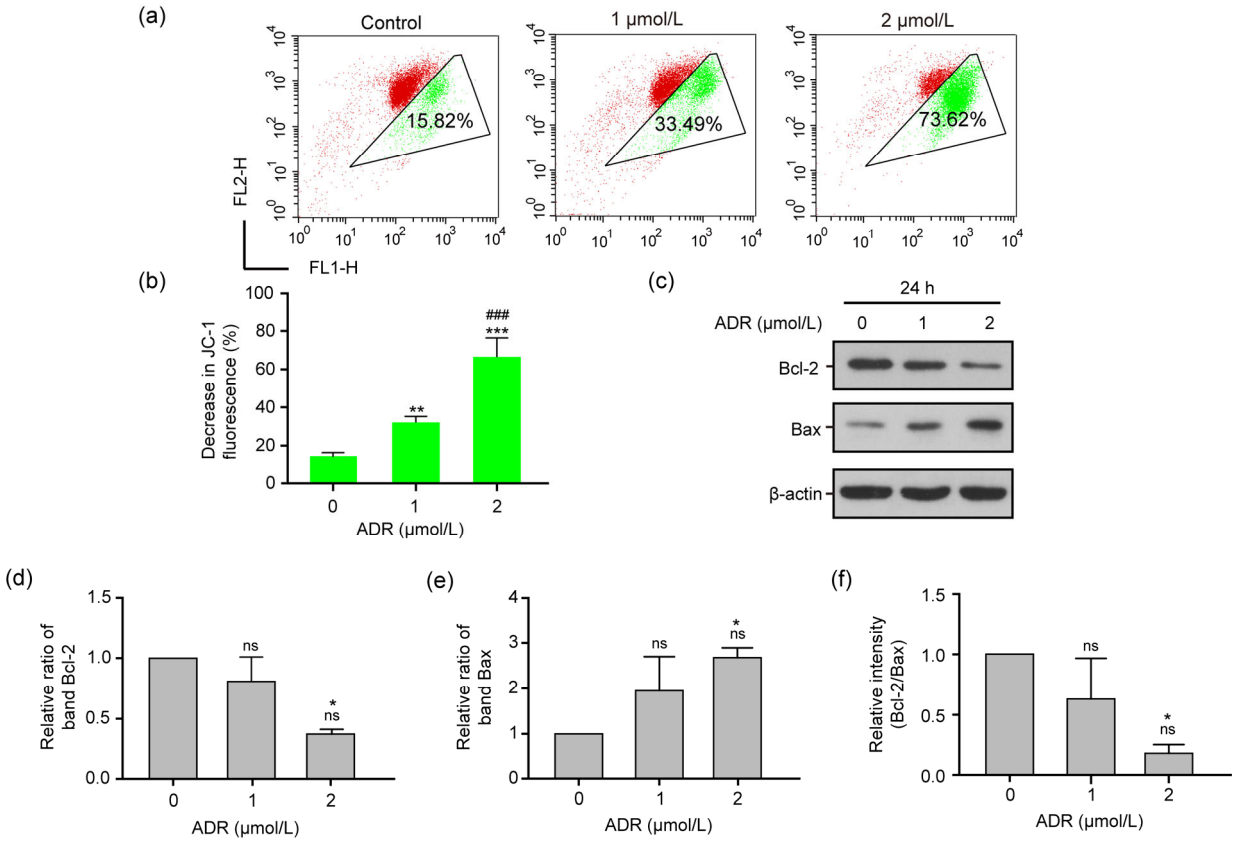

Fig. 5 Mitochondrial function in RPE cells exposed to ADR

(a, b) The levels of mitochondrial membrane potential in ARPE-19 cells exposed to 0, 1, and 2 μmol/L ADR for 24 h. (c–e) The expression levels of the Bcl-2 and Bax proteins of RPE cells exposed to 0, 1, and 2 μmol/L ADR for 24 h by Western blot assay. (f) Bcl-2/Bax ratios of RPE cells exposed to 0, 1, and 2 μmol/L ADR for 24 h by Western blot assay. Data are expressed as mean±SD (n=3). $^{*}P$<0.05, $^{**}P$<0.01, $^{***}P$<0.001, as compared with the control group; $^{\#\#\#}P$<0.001, as compared with the 1 μmol/L ADR group; ns (not significant): 1 μmol/L ADR vs. control, or 2 μmol/L ADR vs. 1 μmol/L ADR

signaling pathway are involved in DNA damage. To further elucidate the primary mechanism of ADR-induced ARPE-19 cell apoptosis, the γ-H2AX assay was used to assess DNA damage. Figs. 7a and 7b demonstrate that the γ-H2AX protein expression levels in ARPE-19 cells exposed to 2 μmol/L ADR for 24 h increased with the dose, as compared to the control group (P<0.001). The accumulation of γ-H2AX foci in the nucleus in ARPE-19 cells exposed to 1 and 2 μmol/L ADR for 6 h was significantly elevated as observed by immunofluorescence (P<0.01, Figs. 7e and 7f), in comparison to the control group. In addition, Figs. 7a, 7c, and 7d show that the protein expression levels of p-CHK1 and p-CHK2 in ARPE-19 cells exposed to 1 or 2 μmol/L ADR for 24 h were significantly enhanced, as compared with the control group (P<0.01 or P<0.001).

4 Discussion

RPE cells, which dedifferentiate and migrate through a retinal break and proliferate on the retinal surface, are used in PVR pathogenesis studies (Leaver, 1995). Previous studies have focused on the role of anticancer drugs as effective inhibitors of RPE proliferation (Sunalp et al., 1984). ADR is one of the most widely used agents in experimental and clinical studies, and it has a proven anti-proliferative effect in PVR. ADR can attenuate the severity of PVR in animal models (Kuo et al., 2012) and decrease vitreous and retinal proliferative response in patients (Rong and Li, 2002). Previous studies have indicated that ADR therapy may possess potential value in PVR treatment; however, the accurate signal transduction involved is unclear and requires further research.

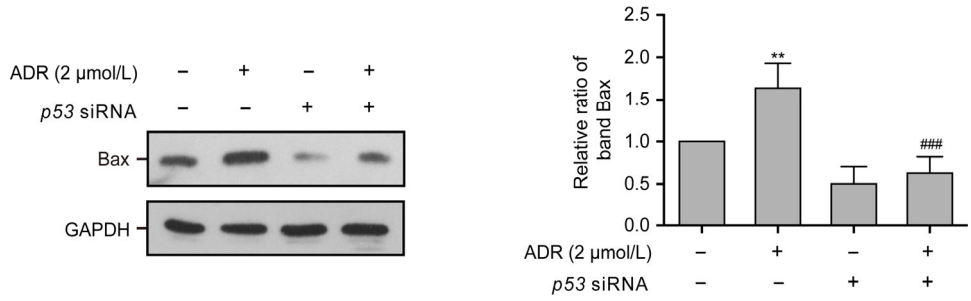

Fig. 6 Bax protein expression in ARPE-19 cells exposed to ADR, *p53* siRNA, and ADR plus *p53* siRNA for 24 h
Data are expressed as mean±SD (n=3). $^{**}P$<0.01, as compared with the control group; $^{###}P$<0.001, as compared with the 2 μmol/L ADR group

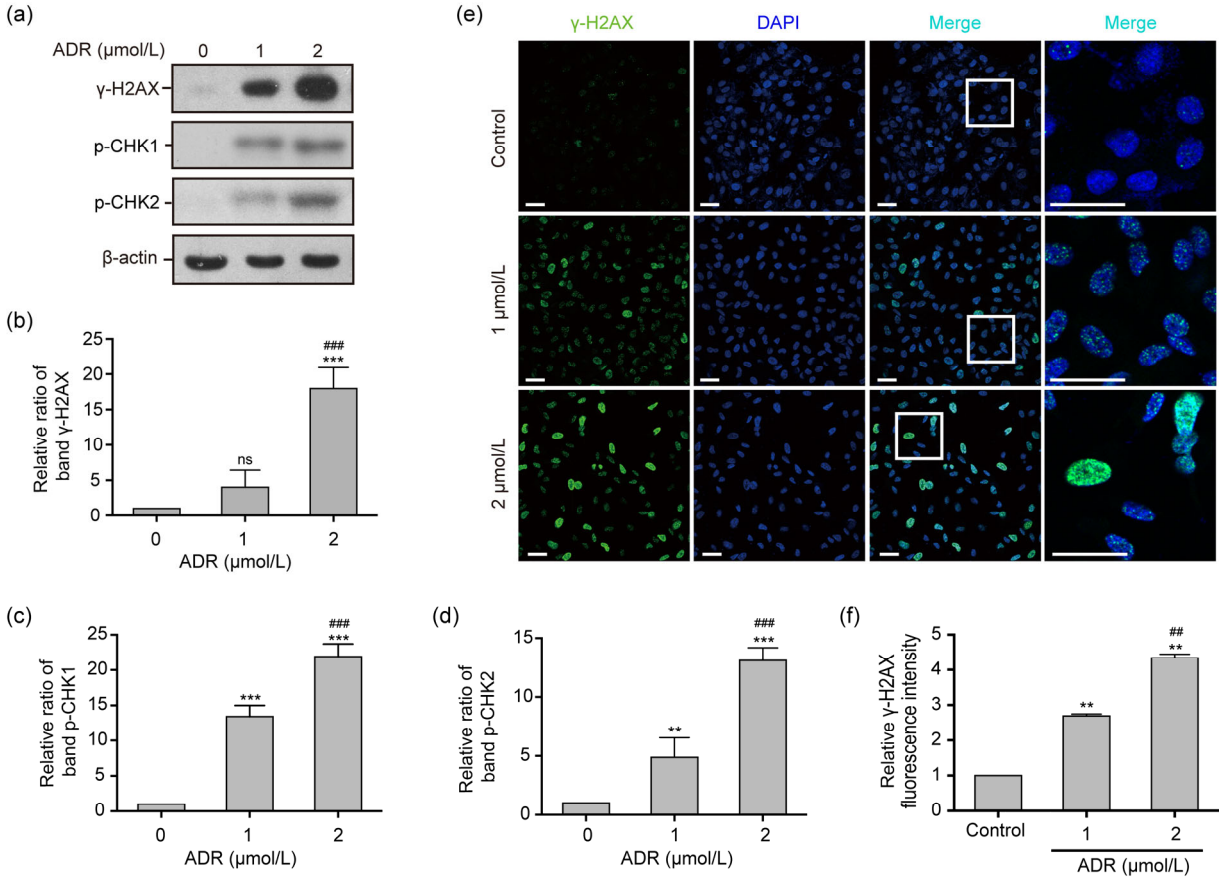

Fig. 7 γ-H2AX assay and the expression levels of the γ-H2AX, p-CHK1, and p-CHK2 proteins in ADR-treated ARPE-19 cells
(a–d) The expression levels of the γ-H2AX, p-CHK1, and p-CHK2 proteins in ARPE-19 cells exposed to 0, 1, and 2 μmol/L ADR for 24 h. (e, f) The fluorescence intensity of γ-H2AX foci (blue, nucleus; green, γ-H2AX foci) in ARPE-19 cells exposed to 0, 1, and 2 μmol/L ADR for 6 h. Scale bar: 50 μm. Data are expressed as mean±SD (n=3). $^{**}P$<0.01, $^{***}P$<0.001, as compared with the control group; $^{##}P$<0.01, $^{###}P$<0.001, as compared with the 1 μmol/L ADR group; ns (not significant): 1 μmol/L ADR vs. control

The caspase pathway is important in regulating cell fate, such as cell proliferation and differentiation, and survival or apoptosis (Savitskaya and Onishchenko, 2015). Data from the caspase analysis in the present study demonstrated that c-caspase-3 levels in ARPE-19 cells exposed to ADR were significantly elevated. Meanwhile, the apoptotic rates were elevated with the ADR dose and exposure time. Thus, caspase-dependent apoptosis was initiated in ADR-treated ARPE-19 cells.

A microarray analysis is a broadly used biotechnology for discovering gene expression patterns (Brazma et al., 2001). With the help of a microarray pathway analysis, we can possibly screen out altered molecular processes. We identified more than 6000 DEGs by simply calculating the fold change of genes, which might be a limitation of the current research. According to a previous report (Consortium et al., 2006), both the fold change and *P*-value of the statistical analysis should be used as criteria for selecting DEGs, which suggests that more biological replicates should be involved for a microarray analysis. The results of our KEGG pathway analysis indicated that the p53 signaling pathway was involved in ADR-induced ARPE-19 apoptosis. Furthermore, a protein–protein interaction analysis identified that the TP53 protein plays a role in binding to target proteins and is involved in DNA damage and oxidative stress. Our study confirmed the relationship between the p53 signaling pathway and ADR-induced RPE apoptosis, and it provided insight into the ADR-dependent mechanisms involved in the pathology of PVR.

In our investigation, the apoptotic rate of ARPE-19 cells exposed to ADR was decreased through the transfection of *p53* siRNA. The expression levels of c-caspase-3 in ARPE-19 cells exposed to ADR plus *p53* siRNA were significantly decreased, as *p*53 was presumed to be the up-stream signaling molecule of caspase that significantly induces the apoptotic response in ADR-treated RPE cell models.

According to the results of the protein–protein interaction analysis, a strong relationship between DNA damage and the p53 signaling pathway exists. In addition, ADR is a well-known inducer of DNA damage to inhibit cancer cell proliferation (Tewey et al., 1984); it promotes DDS breaks during replication and creates DNA damage (Christmann and Kaina, 2013). Generally, DNA damage activates sensors, such as γ-H2AX, and motivates the mediator protein p53 (Polo and Jackson, 2011). In the present study, DNA lesions were found in RPE cells during the early stages following ADR treatment, along with increased expressions and aggregations of γ-H2AX foci in the nucleus. In principle, the cells use different strategies, including DNA repair in response to DNA damage (Tanaka et al., 2000). The DNA damage-responsive kinases ataxia telangiectasia mutated (ATM) and ATM- and Rad3-related (ATR), as well as their downstream mediators CHK1 and CHK2, activated the p53 pathway (Matt and Hofmann, 2016). The present study found that in RPE cells exposed to ADR, the initiation of DNA damage and the promotion of DNA repair occurred simultaneously. In addition, the expression levels of the p-CHK1 and p-CHK2 proteins were significantly enhanced, as stated above. It can be inferred that DNA damage triggers p53 signaling activation in ARPE-19 cells exposed to ADR.

The protein–protein interaction assay showed that the TP53 protein is linked to oxidative stress, which can induce apoptotic death, where the mitochondria play a central role in the apoptotic cascade. ADR-activated downstream genes, such as *Bax*, cause mitochondria-dependent cancer cell apoptosis (Flores et al., 2002; Wang et al., 2004; Deus et al., 2015). In our study, the expression level of *Bax* in cells exposed to ADR was decreased by *p53* siRNA (*p53* knockdown), thereby demonstrating that mitochondrial dysfunction was reversed. Reportedly, p53 causes mitochondrial membrane depolarization and caspase activation during apoptosis (Marchenko et al., 2000; Vaseva et al., 2012). The results of the JC-1 assay showed that RPE mitochondrial dysfunction occurred before apoptosis, indicating that mitochondria-dependent apoptosis was regulated by the classic p53 pathway in ADR-treated ARPE-19 cells. Presumably, caspase-dependent apoptosis was mediated by p53-dependent mitochondrial dysfunction in ADR-induced ARPE-19 cells.

This study used high-throughput technology to expose the mechanism of action of ADR on RPE cells, elucidate the related signaling pathways and molecules, and provide a better target for the treatment of PVR. Although the above-mentioned results suggest that the p53 pathway plays an important role in ADR-induced apoptosis in RPE cells, the results of in vitro experiments may not be extrapolated to in vivo

experiments and human trials. Performing animal experiments and human trials will be important for validating our findings.

5 Conclusions

In summary, the present study applied a transcriptomic approach to investigate the mechanisms of ADR-induced ARPE-19 cell apoptosis. As shown in Fig. 8, our results demonstrated that p53-dependent mitochondrial dysfunction regulates caspase-dependent apoptosis, and the p53 signaling pathway can be activated by DNA damage in ARPE-19 cells exposed to ADR. Based on the results of clinical studies, ADR may be effective in preventing PVR in the early stage of retinal detachment and for treating PVR.

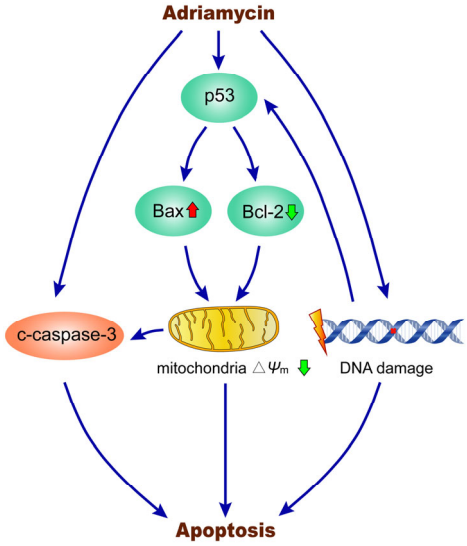

Fig. 8 Mechanisms of ADR-induced ARPE-19 cell apoptosis

Upon treatment with ADR, the expression of p53 can be activated. The p53 downstream mitochondria-related genes *Bax* and *Bcl-2* can be up-regulated and down-regulated, respectively, further decreasing the mitochondrial membrane potential ($\Delta\Psi_m$) and regulating caspase-dependent apoptosis. Simultaneously, the p53 signaling pathway can be activated by DNA damage in ARPE-19 cells exposed to ADR, leading to apoptosis

Compliance with ethics guidelines

Yu-chen LIN, Ze-ren SHEN, Xiao-hui SONG, Xin LIU, and Ke YAO declare that they have no conflict of interest.

This article does not contain any studies with human or animal subjects performed by any of the authors.

References

Amarnani D, Machuca-Parra AI, Wong LL, et al., 2017. Effect of methotrexate on an in vitro patient-derived model of proliferative vitreoretinopathy. *Invest Ophthalmol Vis Sci*, 58(10):3940-3949. https://doi.org/10.1167/iovs.16-20912

Asaria RHY, Kon CH, Bunce C, et al., 2001. Adjuvant 5-fluorouracil and heparin prevents proliferative vitreoretinopathy: results from a randomized, double-blind, controlled clinical trial. *Ophthalmology*, 108(7):1179-1183. https://doi.org/10.1016/S0161-6420(01)00589-9

Brazma A, Hingamp P, Quackenbush J, et al., 2001. Minimum information about a microarray experiment (MIAME)-toward standards for microarray data. *Nat Genet*, 29(4):365-371. https://doi.org/10.1038/ng1201-365

Charteris DG, Sethi CS, Lewis GP, et al., 2002. Proliferative vitreoretinopathy-developments in adjunctive treatment and retinal pathology. *Eye (Lond)*, 16(4):369-374. https://doi.org/10.1038/sj.eye.6700194

Charteris DG, Aylward GW, Wong D, et al., 2004. A randomized controlled trial of combined 5-fluorouracil and low-molecular-weight heparin in management of established proliferative vitreoretinopathy. *Ophthalmology*, 111(12):2240-2245. https://doi.org/10.1016/j.ophtha.2004.05.036

Christmann M, Kaina B, 2013. Transcriptional regulation of human DNA repair genes following genotoxic stress: trigger mechanisms, inducible responses and genotoxic adaptation. *Nucleic Acids Res*, 41(18):8403-8420. https://doi.org/10.1093/nar/gkt635

Claes C, Lafetá AP, 2014. Proliferative vitreoretinopathy. *Dev Ophthalmol*, 54:188-195. https://doi.org/10.1159/000360466

Consortium M, Shi L, Reid LH, et al., 2006. The microarray quality control (MAQC) project shows inter- and intraplatform reproducibility of gene expression measurements. *Nat Biotechnol*, 24(9):1151-1161. https://doi.org/10.1038/nbt1239

Daniels SA, Coonley KG, Yoshizumi MO, 1990. Taxol treatment of experimental proliferative vitreoretinopathy. *Graefes Arch Clin Exp Ophthalmol*, 228(6):513-516. https://doi.org/10.1007/BF00918482

Dash SK, Chattopadhyay S, Ghosh T, et al., 2015. Self-assembled betulinic acid protects doxorubicin induced apoptosis followed by reduction of ROS-TNF-α-caspase-3 activity. *Biomed Pharmacother*, 72:144-157. https://doi.org/10.1016/j.biopha.2015.04.017

Deus CM, Zehowski C, Nordgren K, et al., 2015. Stimulating basal mitochondrial respiration decreases doxorubicin apoptotic signaling in H9c2 cardiomyoblasts. *Toxicology*, 334:1-11. https://doi.org/10.1016/j.tox.2015.05.001

di Marco A, Gaetani M, Scarpinato B, 1969. Adriamycin (NSC-123,127): a new antibiotic with antitumor activity. *Cancer Chemother Rep*, 53(1):33-37.

Eibl KH, Fisher SK, Lewis GP, 2009. Alkylphosphocholines: a

new approach to inhibit cell proliferation in proliferative vitreoretinopathy. *Dev Ophthalmol*, 44:46-55. https://doi.org/10.1159/000223945

Flores ER, Tsai KY, Crowley D, et al., 2002. p63 and p73 are required for p53-dependent apoptosis in response to DNA damage. *Nature*, 416(6880):560-564. https://doi.org/10.1038/416560a

Heimann H, Bartz-Schmidt KU, Bornfeld N, et al., 2007. Scleral buckling versus primary vitrectomy in rhegmatogenous retinal detachment: a prospective randomized multicenter clinical study. *Ophthalmology*, 114(12):2142-2154. https://doi.org/10.1016/j.ophtha.2007.09.013

Kumar A, Nainiwal S, Choudhary I, et al., 2002. Role of daunorubicin in inhibiting proliferative vitreoretinopathy after retinal detachment surgery. *Clin Exp Ophthalmol*, 30(5):348-351. https://doi.org/10.1046/j.1442-9071.2002.00554.x

Kuo HK, Wu PC, Yang PM, et al., 2007. Effects of topoisomerase II inhibitors on retinal pigment epithelium and experimental proliferative vitreoretinopathy. *J Ocul Pharmacol Ther*, 23(1):14-20. https://doi.org/10.1089/jop.2006.0059

Kuo HK, Chen YH, Wu PC, et al., 2012. Attenuated glial reaction in experimental proliferative vitreoretinopathy treated with liposomal doxorubicin. *Invest Ophthalmol Vis Sci*, 53(6):3167-3174. https://doi.org/10.1167/iovs.11-7972

Leaver PK, 1995. Proliferative vitreoretinopathy. *Br J Ophthalmol*, 79(10):871-872. https://doi.org/10.1136/bjo.79.10.871

Leiderman YI, Miller JW, 2009. Proliferative vitreoretinopathy: pathobiology and therapeutic targets. *Semin Ophthalmol*, 24(2):62-69. https://doi.org/10.1080/08820530902800082

Lisenko K, Dingeldein G, Cremer M, et al., 2017. Addition of rituximab to CHOP-like chemotherapy in first line treatment of primary mediastinal B-cell lymphoma. *BMC Cancer*, 17:359. https://doi.org/10.1186/s12885-017-3332-3

Machemer R, van Horn D, Aaberg TM, 1978. Pigment epithelial proliferation in human retinal detachment with massive periretinal proliferation. *Am J Ophthalmol*, 85(2):181-191. https://doi.org/10.1016/S0002-9394(14)75946-X

Marchenko ND, Zaika A, Moll UM, 2000. Death signal-induced localization of p53 protein to mitochondria. A potential role in apoptotic signaling. *J Biol Chem*, 275(21):16202-16212.

Martins-Neves SR, Paiva-Oliveira DI, Wijers-Koster PM, et al., 2016. Chemotherapy induces stemness in osteosarcoma cells through activation of Wnt/β-catenin signaling. *Cancer Lett*, 370(2):286-295. https://doi.org/10.1016/j.canlet.2015.11.013

Matt S, Hofmann TG, 2016. The DNA damage-induced cell death response: a roadmap to kill cancer cells. *Cell Mol Life Sci*, 73(15):2829-2850. https://doi.org/10.1007/s00018-016-2130-4

Minotti G, Menna P, Salvatorelli E, et al., 2004. Anthracyclines: molecular advances and pharmacologic developments in antitumor activity and cardiotoxicity. *Pharmacol Rev*, 56(2):185-229. https://doi.org/10.1124/pr.56.2.6

Moritera T, Ogura Y, Yoshimura N, et al., 1992. Biodegradable microspheres containing adriamycin in the treatment of proliferative vitreoretinopathy. *Invest Ophthalmol Vis Sci*, 33(11):3125-3130.

Patel N, Garikapati KR, Pandita RK, et al., 2017. miR-15a/miR-16 down-regulates BMI1, impacting Ub-H2A mediated DNA repair and breast cancer cell sensitivity to doxorubicin. *Sci Rep*, 7(1):4263. https://doi.org/10.1038/s41598-017-02800-2

Polo SE, Jackson SP, 2011. Dynamics of DNA damage response proteins at DNA breaks: a focus on protein modifications. *Genes Dev*, 25(5):409-433. https://doi.org/10.1101/gad.2021311

Rong A, Li J, 2002. Intravitreal injection of doxorobicin and dexamethason in treatment of proliferative vitreoretinopathy. *Natl Med J China*, 82(8):546-548 (in Chinese). https://doi.org/10.3760/j:issn:0376-2491.2002.08.012

Savitskaya MA, Onishchenko GE, 2015. Mechanisms of apoptosis. *Biochemistry (Mosc)*, 80(11):1393-1405. https://doi.org/10.1134/S0006297915110012

Steinhorst UH, Chen EP, Machemer R, et al., 1993. *N*,*N*-dimethyladriamycin for treatment of experimental proliferative vitreoretinopathy: efficacy and toxicity on the rabbit retina. *Exp Eye Res*, 56(4):489-495. https://doi.org/10.1006/exer.1993.1062

Sunalp M, Wiedemann P, Sorgente N, et al., 1984. Effects of cytotoxic drugs on proliferative vitreoretinopathy in the rabbit cell injection model. *Curr Eye Res*, 3(4):619-623. https://doi.org/10.3109/02713688409003063

Sunalp MA, Wiedemann P, Sorgente N, et al., 1985. Effect of adriamycin on experimental proliferative vitreoretinopathy in the rabbit. *Exp Eye Res*, 41(1):105-115. https://doi.org/10.1016/0014-4835(85)90099-5

Tanaka H, Arakawa H, Yamaguchi T, et al., 2000. A ribonucleotide reductase gene involved in a p53-dependent cell-cycle checkpoint for DNA damage. *Nature*, 404(6773):42-49. https://doi.org/10.1038/35003506

Tewey KM, Rowe TC, Yang L, et al., 1984. Adriamycin-induced DNA damage mediated by mammalian DNA topoisomerase II. *Science*, 226(4673):466-468. https://doi.org/10.1126/science.6093249

van Bockxmeer FM, Martin CE, Thompson DE, et al., 1985. Taxol for the treatment of proliferative vitreoretinopathy. *Invest Ophthalmol Vis Sci*, 26(8):1140-1147.

Vaseva AV, Marchenko ND, Ji K, et al., 2012. p53 opens the mitochondrial permeability transition pore to trigger necrosis. *Cell*, 149(7):1536-1548. https://doi.org/10.1016/j.cell.2012.05.014

Wang J, Nachtigal MW, Kardami E, et al., 2013. FGF-2 protects cardiomyocytes from doxorubicin damage via protein

kinase C-dependent effects on efflux transporters. *Cardiovasc Res*, 98(1):56-63. https://doi.org/10.1093/cvr/cvt011

Wang SW, Konorev EA, Kotamraju S, et al., 2004. Doxorubicin induces apoptosis in normal and tumor cells via distinctly different mechanisms: intermediacy of H_2O_2- and p53-dependent pathways. *J Biol Chem*, 279(24): 25535-25543. https://doi.org/10.1074/jbc.M400944200

Wang ZC, Wang J, Xie RF, et al., 2015. Mitochondria-derived reactive oxygen species play an important role in doxorubicin-induced platelet apoptosis. *Int J Mol Sci*, 16(5):11087-11100. https://doi.org/10.3390/ijms160511087

Wickham L, Bunce C, Wong D, et al., 2007. Randomized controlled trial of combined 5-fluorouracil and low-molecular-weight heparin in the management of unselected rhegmatogenous retinal detachments undergoing primary vitrectomy. *Ophthalmology*, 114(4):698-704. https://doi.org/10.1016/j.ophtha.2006.08.042

Wiedemann P, Hilgers RD, Bauer P, et al., 1998. Adjunctive daunorubicin in the treatment of proliferative vitreoretinopathy: results of a multicenter clinical trial. *Am J Ophthalmol*, 126(4):550-559. https://doi.org/10.1016/S0002-9394(98)00115-9

Xu XD, Zhao Y, Zhang M, et al., 2017. Inhibition of autophagy by deguelin sensitizes pancreatic cancer cells to doxorubicin. *Int J Mol Sci*, 18(2):370. https://doi.org/10.3390/ijms18020370

Zhao LF, Shan YJ, Liu B, et al., 2017. Functional screen analysis reveals miR-3142 as central regulator in chemoresistance and proliferation through activation of the PTEN-AKT pathway in CML. *Cell Death Dis*, 8(5): e2830. https://doi.org/10.1038/cddis.2017.223

List of electronic supplementary materials

Fig. S1 Gene ontology (GO) enrichment analysis of all the differentially expressed genes

中文概要

题　目：比较转录组学分析揭示阿霉素经 p53 信号通路诱导视网膜色素上皮细胞凋亡

目　的：通过比较阿霉素（ADR）作用的视网膜色素上皮细胞（ARPE-19）和正常 ARPE-19 间的差异表达基因和信号通路，探究 ADR 治疗玻璃体视网膜增殖性疾病的潜在机制。

创新点：首次运用基因芯片技术通过比较转录组学分析探究 ADR 促进 ARPE-19 细胞凋亡的机制。

方　法：采用磺酰罗丹明 B（sulforhodamine B，SRB）比色法和碘化丙啶（PI）单染结合流式细胞术检测 ADR 对 ARPE-19 细胞的增殖抑制作用；通过基因芯片技术筛选 ADR 作用的 ARPE-19 细胞（实验组）和正常 ARPE-19 细胞（对照组）间的差异表达基因和相关信号通路；用 JC-1 染色结合流式细胞术和 Bcl2/Bax 蛋白表达比率检测线粒体功能；通过检测 γ-H2AX、p-CHK1、p-CHK2 等蛋白表达量分析 DNA 的损伤和修复。

结　论：ADR 通过启动 DNA 损伤反应，引起 p53 信号通路依赖的线粒体功能失调并激活 caspase 依赖的凋亡，最终导致 ARPE-19 细胞死亡。

关键词：阿霉素；玻璃体视网膜增殖性疾病；视网膜色素上皮层；p53；凋亡